

SegACIL: Solving the Stability-Plasticity Dilemma in Class-Incremental Semantic Segmentation

Jiaxu Li^{1*}, Songning Lai^{2*}, Rui Li^{1,5*}, Di Fang³, Kejia Fan¹, Jianheng Tang⁴,
Yuhan Zhao¹, Rongchang Zhao¹, Dongzhan Zhou⁵, Yutao Yue², Huiping Zhuang^{3†}

¹Central South University, ²The Hong Kong University of Science and Technology (Guangzhou),

³South China University of Technology, ⁴Peking University, ⁵Shanghai Artificial Intelligence Laboratory

Abstract—While deep learning has made remarkable progress in recent years, models continue to struggle with catastrophic forgetting when processing continuously incoming data. This issue is particularly critical in continual learning, where the balance between retaining prior knowledge and adapting to new information-known as the stability-plasticity dilemma-remains a significant challenge. In this paper, we propose *SegACIL*, a novel continual learning method for semantic segmentation based on a *linear closed-form solution*. Unlike traditional methods that require multiple epochs for training, *SegACIL* only requires a *single epoch*, significantly reducing computational costs. Furthermore, we provide a theoretical analysis demonstrating that *SegACIL* achieves performance on par with joint learning, effectively retaining knowledge from previous data which makes it to keep both stability and plasticity at the same time. Extensive experiments on the Pascal VOC2012 dataset show that *SegACIL* achieves superior performance in the sequential, disjoint, and overlap settings, offering a robust solution to the challenges of class-incremental semantic segmentation. Code is available at <https://github.com/qwrawq/SegACIL>.

Index Terms—Analytic learning, class-incremental learning, continual learning, semantic segmentation

I. INTRODUCTION

Deep learning has made substantial progress across a variety of domains in computer vision. However, one critical challenge in real-world applications is the continuous arrival of new data, which requires the models to learn incrementally over time [1]. A simple method is to retrain models using the complete dataset, but this process is both time-consuming and resource-intensive, leading to considerable wastage of computational and financial resources [2]. Moreover, past data may become unavailable due to privacy concerns, further complicating retraining efforts. An alternative approach is to train models directly on newly arriving data, yet this strategy is often plagued by catastrophic forgetting [3], where the model forgets previously acquired knowledge when adapting to new information. To address this issue, continual learning techniques are proposed to mitigate the effects of forgetting while allowing models to adapt to new data in an incremental fashion [4].

A challenge in continual learning is the stability-plasticity dilemma [3], which involves balancing two conflicting goals: stability and plasticity. Stability refers to a model’s ability to retain knowledge from past tasks, while plasticity requires the

model to adapt to new incoming data. Striking the right balance is essential for successful continual learning.

Existing continual learning methods primarily focus on tasks such as image classification [5], object detection [6], and semantic segmentation [7], [8]. Class-incremental semantic segmentation (CSS), however, presents unique challenges. Unlike traditional semantic segmentation, which operates on a fixed set of classes, and unlike image-level tasks, such as classification, which operate at a more abstract level, CSS involves pixel-level granularity, making it particularly vulnerable to catastrophic forgetting [3] where the model loses its ability to segment earlier classes when learning new ones. Additionally, the approach must effectively manage class relationships and contextual information to avoid disrupting overall segmentation performance. These complexities have spurred significant research into tailored continual learning strategies for CSS.

Recent advancements in CSS can be roughly classified into exemplar-free and exemplar-replay approaches. Exemplar-free methods aim to retain knowledge from previously encountered data without storing explicit exemplars. These methods often employ self-supervised learning [9], regularization techniques [7], [8], or dynamic network architectures [10], [11]. Exemplar-replay methods, on the other hand, rely on strategies such as sample replay, feature replay, and auxiliary dataset integration [12], or pseudo-data generated by generative models [13]. While these methods have shown promise in retaining knowledge over time, they still face challenges in terms of computational efficiency and memory usage.

To address these issues, we propose **SegACIL**, a novel method that leverages a linear closed-form solution for CSS. Unlike existing methods that require multiple epochs to achieve incremental learning, *SegACIL* requires only a single epoch training, significantly reducing both time and financial costs. Our method ensures complete knowledge retention without forgetting, making it highly efficient and suitable for real-world applications. Furthermore, *SegACIL* incorporates theoretical advancements from analytic learning, which has recently gained traction as an alternative to conventional gradient-based methods [14]. By directly calculating neural network parameters, analytic learning methods overcome key challenges associated with back-propagation, including gradient vanishing and the instability of iterative training processes [14], [15]. These methods have been applied to various domains, including images [15]–[17] and time series [18] classification, few-shot

The first three authors contributed equally to this work.

†Corresponding author: hpzhuang@scut.edu.cn.

learning [19], long-tailed learning [20], [21], federated learning [22] and reinforcement learning [23]. Drawing inspiration from recent advancements, SegACIL, a system for CSS, leverages analytic learning to tackle the stability-plasticity dilemma, thereby achieving superior performance in its domain.

We further propose a pseudo-labeling technique to address the semantic drift issue, which occurs when previously learned categories are labeled as background in subsequent steps across both the disjoint, and overlap settings. Extensive experiments on the Pascal VOC2012 dataset [24] demonstrate that SegACIL outperforms existing methods, achieving superior performance across all three settings: sequential, disjoint, and overlap.

In summary, the contributions of this paper are as follows: **(i)** We introduce an analytical learning-based framework designed for CSS; **(ii)** we incorporated a pseudo-labeling technique into our framework to address the semantic drift in the disjoint and overlap settings. **(iii)** we provide theoretical proof that SegACIL achieves performance on par with joint learning in continual learning, validated through extensive experiments on the Pascal VOC2012 dataset, outperforming current advanced methods in CSS.

II. PROBLEM DEFINITION AND SETUPS

A. Preliminaries

To introduce our proposed strategies, we begin by defining the semantic segmentation task, which aims to assign a class label to each pixel in an image. The input image space is represented as $\mathcal{U} \in \mathbb{R}^{H \times W \times 3}$, where H and W denote the spatial dimensions. The set of possible classes is $\mathcal{C} = \{c_i\}_{i=0}^{C-1}$, and the output space, representing the segmentation map, is $\mathcal{V} \in \mathcal{C}^{H \times W}$. Given a training dataset $\mathcal{T} = \{(\mathbf{u}_n, \mathbf{v}_n)\}_{n=1}^N$, where each pair $(\mathbf{u}_n, \mathbf{v}_n) \in \mathcal{U} \times \mathcal{V}$, the objective is to learn a mapping function M that predicts a pixel-wise class probability distribution: $M: \mathcal{U} \rightarrow \mathbb{R}^{H \times W \times C}$. The segmentation mask is subsequently computed as: $\hat{\mathbf{v}}_n = \arg \max_{c \in \mathcal{C}} M(\mathbf{u}_n)[h, w, c]$, where $h = 1, \dots, H$, $w = 1, \dots, W$, and $M(\mathbf{u}_n)[h, w, c]$ indicates the probability of pixel (h, w) belonging to class c . In practice, M is often implemented as an autoencoder composed of an encoder E and a classifier Φ .

In the traditional supervised learning paradigm, the entire training set \mathcal{T} is available at once, and the model is trained in a single step. However, in the context of continual learning, training occurs iteratively, with each step introducing new categories alongside a subset of the training data. This process spans multiple steps, denoted as $\{\text{Step-1}, \text{Step-2}, \dots, \text{Step-T}\}$. At step t , the label set \mathcal{C}_{t-1} is expanded by adding a new set of categories \mathcal{S}_t , resulting in an updated label set $\mathcal{C}_t = \mathcal{C}_{t-1} \cup \mathcal{S}_t$. Concurrently, a new training subset $\mathcal{T}_t \subset \mathcal{U} \times \mathcal{C}_t$ is introduced, which is used to update the previous model M_{t-1} to M_t . At step $t = 1$, a standard supervised training procedure is applied to a subset of data and classes. Following the principles of incremental class learning, it is assumed that the newly introduced class sets are mutually exclusive, except for the background class c_0 , *i.e.*, $\mathcal{S}_i \cap \mathcal{S}_j = \{c_0\}$.

In CSS, the aim is to learn a mapping function M , parameterized by θ_t , using the newly introduced data $\mathcal{T}_t =$

$\{(\mathbf{u}_n^t, \mathbf{v}_n^t)\}_{n=1}^{N^t}$. The goal is to minimize the model's loss on \mathcal{T}_t while preserving its performance on previously learned tasks. This requires balancing the model's plasticity for learning new tasks and its stability for retaining prior knowledge. The universal optimization objective in CSS is expressed as:

$$\min_{\theta_t} [\lambda_1 \mathcal{L}_{base}(\theta_t, \theta_{t-1}, \mathcal{T}_t, \mathcal{C}_{t-1}) + \lambda_2 \mathcal{L}_{new}(\theta_t, \mathcal{T}_t, \mathcal{C}_t)], \quad (1)$$

where \mathcal{L}_{new} measures the loss for new tasks, while \mathcal{L}_{base} ensures that the updated model θ^t retains knowledge from the previous model θ^{t-1} . The coefficients λ_1 and λ_2 control the trade-off between retaining prior knowledge and learning new categories.

Different learning settings are considered for CSS, depending on the availability and labeling of categories during incremental learning. These settings—sequential, disjoint, and overlap—are detailed below.

B. Incremental Learning Settings

Sequential Setting. In the sequential setting, labels for both previously learned and newly introduced categories are available simultaneously during each incremental learning step. This scenario reduces ambiguity as all categories are explicitly labeled, making it relatively straightforward.

Disjoint Setting. The disjoint setting introduces complexity by labeling previously learned categories as background in the current task. This phenomenon, known as semantic drift, challenges the model to differentiate between real background and previously learned classes. Consequently, this setting is more challenging than the sequential setting.

Overlap Setting. The overlap setting further complicates the learning process. Here, only new categories and the background are labeled, but the background label can encompass true background, previously learned categories, and future categories that have not yet been introduced. This ambiguity makes the overlap setting the most challenging.

III. METHOD

A. Gradient Descent-Based Training

The overview of our method is shown in (1). First, we use gradient descent to train a regular classifier in the initial training step, which includes multiple training epochs. Theoretically, it can be composed of any commonly network structure with a classifier. The feature map extracted by the encoder is

$$\mathbf{u}^{\text{encoder}} = E(\mathbf{u}), \quad (2)$$

where $\mathbf{u}^{\text{encoder}} \in \mathbb{R}^{H^* \times W^* \times d_{\text{encoder}}}$, H^* and W^* are usually smaller than H and W . Then, the predicted $\hat{\mathbf{v}}$ is obtained through a classification head, *i.e.*

$$\hat{\mathbf{v}} = f_{\text{upsample}}(\Phi \mathbf{u}^{\text{encoder}}), \quad (3)$$

where f_{upsample} upsamples the feature map to the same size as the ground truth \mathbf{v} with the bilinear interpolation operation.

After training, we save and freeze the encoder and treat the encoder as a feature extractor.

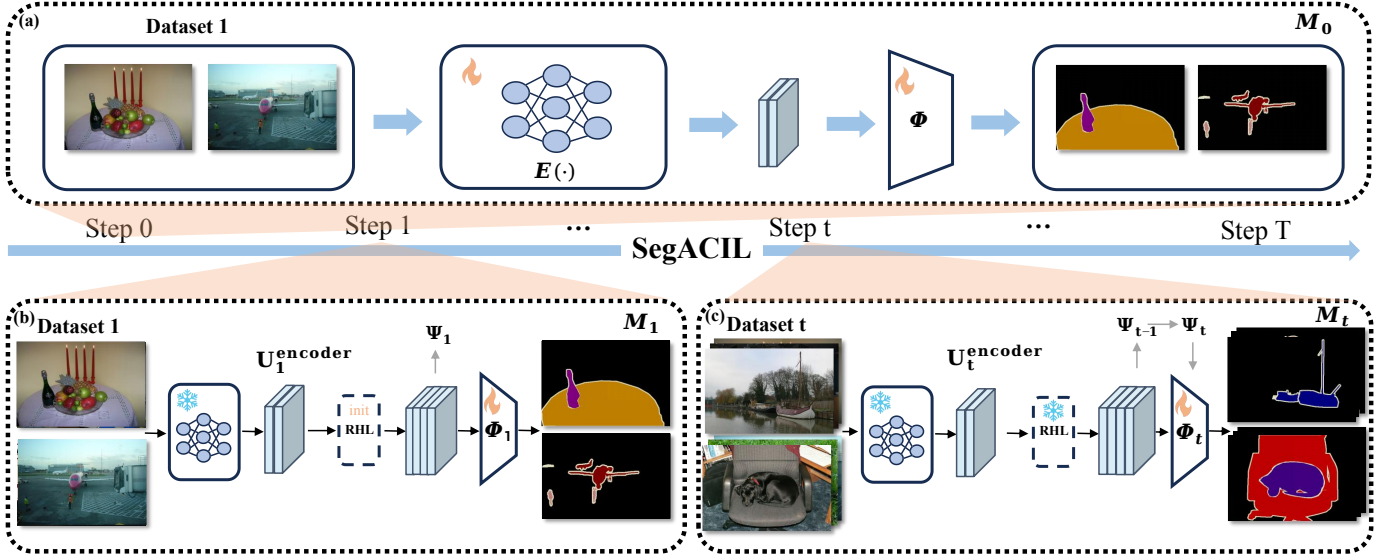


Fig. 1. Schematic Overview of Our Framework. Subfigure (a) illustrates Step 0, showcasing Gradient Descent-Based Training on Dataset 1. Subfigure (b) highlights Step 1, demonstrating Regression-Based Realignment on Dataset 1 to obtain the Ψ_1 and Φ_1 matrices. Finally, Subfigure (c) depicts the general process of incremental learning in SegACIL, specifically the recursive update of the Ψ and Φ matrices.

B. Regression-Based Realignment

After the Gradient Descent-Based Training phase, we transition to the Regression-Based Realignment step. In this stage, the analytical classifier supplants the previous classifier, utilizing the analytical classifier as the foundational mechanism. This step encompasses three main sub-steps:

(i) Feature Extraction. Initially, we generate the feature matrix, denoted as $\mathbf{U}_1^{\text{encoder}}$, by feeding the input tensor $\mathbf{U}_1^{\text{train}}$ through the trained encoder network:

$$\mathbf{U}_1^{\text{encoder}} = E(\mathbf{U}_1^{\text{train}}), \quad (4)$$

where $\mathbf{U}_1^{\text{train}} \in \mathbb{R}^{B \times H \times W}$, $\mathbf{U}_1^{\text{encoder}} \in \mathbb{R}^{N_1 \times d_{\text{encoder}}}$, $N_1 = B \times H^* \times W^*$ and B represents batch size.

(ii) Feature Expansion with RHL. Instead of directly connecting these features to the classification output through a single classifier layer, we introduce a Randomly-initialized Hidden Layer (RHL). This involves expanding the feature matrix $\mathbf{U}_1^{\text{encoder}}$ into $\mathbf{U}_1^{(E)}$ as follows:

$$\mathbf{U}_1^{(E)} = f_{\text{act}}(\mathbf{U}_1^{\text{encoder}} \Phi^E), \quad (5)$$

where $\mathbf{U}_1^{(E)} \in \mathbb{R}^{N_1 \times d_E}$, and d_E signifies the expanded feature dimension (typically $d_{\text{encoder}} < d_E$) and we refer to the expanded feature dimension as the buffer size. Here, f_{act} represents the activation function, and Φ^E is the expansion matrix initialized with elements drawn from a normal distribution.

Role of the RHL. The RHL is essential for enlarging the parameter space, thereby facilitating more effective analytical learning. By projecting the original features into a higher-dimensional space, the RHL enhances the model's ability to detect complex patterns and relationships within the data. This increase in dimensionality allows the model to grasp deeper insights and recognize subtle and intricate connections that may not be apparent in a lower-dimensional setting.

(iii) Linear Regression Mapping. Finally, the expanded features $\mathbf{U}_1^{(E)}$ are used to predict the label matrix $\mathbf{V}_1^{\text{train}}$ through a linear regression approach. This involves solving the following optimization problem:

$$\underset{\Phi_1}{\text{argmin}} (\|\mathbf{V}_1^{\text{train}} - \mathbf{U}_1^{(E)} \Phi_1\|_F^2 + \gamma \|\Phi_1\|_F^2), \quad (6)$$

where γ is a regularization parameter, $\|\cdot\|_F$ is the Frobenius norm, and $\mathbf{V}_1^{\text{train}} \in \mathbb{R}^{N_1 \times d_{C_1}}$ is obtained by applying bilinear interpolation to the ground truth to match the dimensions ($H^* \times W^*$). The optimal solution to this problem is:

$$\hat{\Phi}_1 = (\mathbf{U}_1^{(E)\top} \mathbf{U}_1^{(E)} + \gamma \mathbf{I})^{-1} \mathbf{U}_1^{(E)\top} \mathbf{V}_1^{\text{train}}, \quad (7)$$

where \mathbf{I} is the identity matrix, $^{-1}$ represents the matrix inversion operation, and \top denotes the matrix transpose operation.

C. Class-Incremental Semantic Segmentation Learning

After completing the Regression-Based Realignment, we proceed with the CSS process in a recursive and analytical manner. To demonstrate this, Without loss of generality, let $\mathbf{V}_{1:t-1}^{\text{train}}$, $\mathbf{V}_{1:t}^{\text{train}}$ and $\mathbf{U}_{1:t-1}^{(E)}$, $\mathbf{U}_{1:t}^{(E)}$ be the accumulated label and feature matrices at steps $t-1$ and t , and they are related via

$$\mathbf{V}_{1:t}^{\text{train}} = \begin{bmatrix} \mathbf{V}_{1:t-1}^{\text{train}} & \mathbf{0} \\ \check{\mathbf{V}}_t^{\text{train}} & \check{\mathbf{V}}_t^{\text{train}} \end{bmatrix}, \quad \mathbf{U}_{1:t}^{(E)} = \begin{bmatrix} \mathbf{U}_{1:t-1}^{(E)} \\ \mathbf{U}_t^{(E)} \end{bmatrix}. \quad (8)$$

The block matrix is due to the covered-uncovered partition

$$\mathbf{V}_t^{\text{train}} = [\check{\mathbf{V}}_t^{\text{train}} \quad \check{\mathbf{V}}_t^{\text{train}}], \quad (9)$$

where $\check{\mathbf{V}}_t^{\text{train}} \in \mathbb{R}^{N_t \times d_{C_{t-1}}}$ is the *projected covered matrix* and $\check{\mathbf{V}}_t^{\text{train}} \in \mathbb{R}^{N_t \times (d_{C_t} - d_{C_{t-1}})}$ is the *projected uncovered matrix*. They correspond to segments displaying the appearance of

covered classes and uncovered classes. The learning problem can then be formulated as:

$$\operatorname{argmin}_{\Phi_{t-1}} (\|\mathbf{V}_{1:t-1}^{\text{train}} - \mathbf{U}_{1:t-1}^{(E)} \Phi_{t-1}\|_F^2 + \gamma \|\Phi_{t-1}\|_F^2), \quad (10)$$

according to Eqn (7), at step $t - 1$, we have:

$$\hat{\Phi}_{t-1} = \left(\mathbf{U}_{1:t-1}^{(E)\top} \mathbf{U}_{1:t-1} + \gamma \mathbf{I} \right)^{-1} \mathbf{U}_{1:t-1}^{(E)\top} \mathbf{V}_{1:t-1}^{\text{train}}, \quad (11)$$

where $\hat{\Phi}_{t-1} \in \mathbb{R}^{d_E \times \sum_{i=1}^{t-1} d_{S_i}}$, with the column size expanding as t increases. Let

$$\Psi_{t-1} = \left(\mathbf{U}_{1:t-1}^{(E)\top} \mathbf{U}_{1:t-1}^{(E)} + \gamma \mathbf{I} \right)^{-1} \quad (12)$$

be the inverted auto-correlation matrix, which captures the correlation information from both current and past samples. Building on this, the goal is to compute $\hat{\Phi}_t$ using only $\hat{\Phi}_{t-1}$, Ψ_{t-1} , and the current step's data $\mathbf{U}_t^{\text{train}}$, without involving historical samples such as $\mathbf{U}_{1:t-1}$. The process is formulated as shown in the following theorem.

Theorem 1. *The Φ weights, recursively obtained by*

$$\hat{\Phi}_t = \left[\hat{\Phi}_{t-1} - \Psi_t \mathbf{U}_t^{(E)} \mathbf{U}_t^{(E)\top} \hat{\Phi}_{t-1} + \Psi_t \mathbf{U}_t^{(E)\top} \hat{\mathbf{V}}_t^{\text{train}} - \Psi_t \mathbf{U}_t^{(E)} \mathbf{U}_t^{(E)\top} \hat{\mathbf{V}}_t^{\text{train}} \right] \quad (13)$$

are equivalent to those obtained from Eqn (11) for step t . The matrix Ψ_t can also be recursively updated by

$$\Psi_t = \left(\Psi_{t-1}^{-1} + \mathbf{U}_t^{(E)\top} \mathbf{U}_t^{(E)} \right)^{-1} \quad (14)$$

Proof. See the supplementary materials. \square

As stated in Theorem 1, our framework provides a recursive update for the Φ weights without losing any historical information. First, the base model is trained on the initial dataset (e.g. to compute $\hat{\Phi}_1$), and the CSS process continues using the recursive formulation to obtain $\hat{\Phi}_t$ for $t > 1$.

Absolute Memory and Privacy-Preserving. We theoretically prove that the continual learning performance of SegACIL is equivalent to joint learning, thus achieving absolute memory. At the same time, we do not need to access historical data. Instead, we store all historical information using the Φ matrix and make it impossible to retrieve historical data through reverse engineering from the Φ matrix. This ensures privacy protection, which is important in privacy-sensitive domains.

D. Pseudo-Labels

In both disjoint and overlap settings, previously learned classes are treated as background in the current task, a phenomenon commonly referred to as semantic drift. To address this issue, we adopt the use of pseudo-labels, following the approaches proposed in prior work [28].

The definition of pseudo-labels is formalized as follows:

$$\hat{v}^t = \begin{cases} v^t, & \text{if } v^t \in S_t \\ v^t, & \text{if } (v^t \in c_0) \wedge (\max(\Omega^{t-1}) < \tau) \\ \hat{v}^{t-1}, & \text{if } (v^t \in c_0) \wedge (\max(\Omega^{t-1}) \geq \tau) \end{cases} \quad (15)$$

where $\Omega^{t-1} \in \mathbb{R}^{\mathbf{H} \times \mathbf{W} \times C_{t-1}}$ is the output of the previous model M_{t-1} , and τ is a threshold that determines whether the pixel

labeled as background ($v^t \in c_0$) should adopt pseudo-labels generated by the prior model. This approach mitigates the semantic drift issue in both disjoint and overlap settings.

IV. EXPERIMENTS

Dataset. We selected the Pascal VOC2012 dataset for CSS. It contains 21 classes. This dataset features wild scenes, with 10,582 images used for training and 1,449 images for validation.

CSS Learning Protocol. The classes of the images for the current step include $C_{t-1} \cup S_t$. In each step, we continuously introduce new classes for learning. For $\forall i, \forall j$ and $i \neq j$, it holds that $S_i \cap S_j = \emptyset$. In an m-n setting, the model first learns m classes, and in each subsequent step, it incrementally learns n classes. For the Pascal VOC2012 dataset, we adopted the 15-1 and 15-5 for the sequential setting. And we adopted 15-1 and 10-1 for both the disjoint and overlap settings.

Evaluation Metrics. We use the widely-adopted mean Intersection-over-Union (mIoU) metric to calculate the average IoU value across all classes. To comprehensively evaluate CSS performance, we compute mIoU values separately for initial classes C_1 , incremental classes $C_T - C_1$, and all classes C_T .

Implementation Details. We used DeepLabv3 as the decoder and ResNet101 as the encoder, which was pretrained on ImageNet-1K. For initial training on the Pascal VOC2012 dataset, we set the number of epochs to 50 and the batch size to 16. We employed SGD as the optimizer with a learning rate of 10^{-2} , a momentum of 0.9, and a weight decay of 10^{-4} . A polynomial learning rate schedule was applied. The loss function used was binary cross-entropy (BCE) loss. In the continual learning step, we set the buffer size to 8192, γ to 1, and the threshold for pseudo-labels to 0.6 in both the disjoint and overlap settings, using ReLU as the activation function. The images were resized to 513×513 , and data augmentation followed the practices of previous work, including random scaling, random flipping, and random cropping. All experiments were conducted using PyTorch on an A100 GPU.

A. Results

Stability. As shown in Tables I and II, SegACIL excels in performance on previously learned classes compared to all other methods, highlighting its stability.

Plasticity. As shown in Tables I and II SegACIL also outperforms most other methods in incremental learning classes, demonstrating its plasticity.

Why SegACIL solves the stability-Plasticity Dilemma? The underlying reason is detailed in Theorem 1, which proves that the continual learning performance is equivalent to joint learning, ensuring absolute memory. This property is further reflected in the results for the sequential 15-1 and 15-5 settings, which are identical.

B. Ablation Studies

Buffer Size Analysis. In the sequential 15-1 setting, we fix $\gamma = 1$ and choose different buffer sizes. The mIoU increases with buffer size shown in Figure 2. A larger buffer size also implies higher computational cost, necessitating a trade-off.

TABLE I
CLASS-INCREMENTAL CSS QUANTITATIVE COMPARISON ON PASCAL VOC2012 IN mIoU (%) UNDER *sequential* SETTING. THE RESULTS OF THE COMPARISON METHOD ARE DIRECTLY TAKEN FROM THE ORIGINAL WORK AND [3]. FOR THE BEST RESULTS, WE USE **BOLD** FORMATTING.

	Method	Year	Model	15-1 (6 steps)			15-5 (2 steps)		
				0-15	16-20	all	0-15	16-20	all
Sequential	<i>fine tuning</i>	-	DeepLabv3+	49.0	17.8	41.6	62.0	38.1	56.3
	LwF [5]	TPAMI2018	DeepLabv3+	33.7	13.7	29.0	68.0	43.0	62.1
	LwF-MC [25]	CVPR2017	DeepLabv3+	12.1	1.9	9.7	70.6	19.5	58.4
	ILT [7]	ICCVW2019	DeepLabv3+	49.2	30.3	48.3	71.3	47.8	65.7
	CIL [26]	ITSC2020	DeepLabv3+	52.4	22.3	45.2	63.8	39.8	58.1
	MiB [8]	CVPR2020	DeepLabv3+	35.7	11.0	29.8	73.0	44.4	66.1
	SDR [27]	CVPR2021	DeepLabv3+	58.5	10.1	47.0	73.6	46.7	67.2
	SDR+MiB [27]	CVPR2021	DeepLabv3+	58.1	11.8	47.1	74.6	43.8	67.3
	SegACIL (Ours)		DeepLabv3	78.1	42.0	70.0	78.1	42.0	70.0

TABLE II
CLASS-INCREMENTAL CSS QUANTITATIVE COMPARISON ON PASCAL VOC2012 IN mIoU (%) UNDER *disjoint* AND *overlapped* SETTINGS. THE RESULTS OF THE COMPARISON METHOD ARE DIRECTLY TAKEN FROM THE ORIGINAL WORK AND [3]. FOR THE BEST RESULTS WE USE **BOLD** FORMATTING.

	Method	Year	Model	15-1 (6 steps)			10-1 (11 steps)		
				0-15	16-20	all	0-10	11-20	all
Disjoint	<i>fine tuning</i>	-	DeepLabv3	0.20	1.80	0.60	6.30	1.10	3.80
	MiB [8]	CVPR2020	DeepLabv3	46.20	12.90	37.90	9.50	4.10	6.90
	PLOP [28]	CVPR2021	DeepLabv3	57.86	13.67	46.48	9.70	7.00	8.40
	SDR [27]	CVPR2021	DeepLabv3+	59.40	14.30	48.70	17.30	11.00	14.30
	RCIL [29]	CVPR2022	DeepLabv3	66.10	18.20	54.70	30.60	4.70	18.20
	SegACIL(Ours)		DeepLabv3	77.66	40.33	68.77	70.85	42.13	57.17
	Overlapped	<i>fine tuning</i>	-	DeepLabv3	0.20	1.80	0.60	6.30	2.80
EWC [30]		PNAS2017	DeepLabv3	0.30	4.30	1.30	-	-	-
LwF-MC [25]		CVPR2017	DeepLabv3	6.40	8.40	6.90	4.65	5.90	4.95
ILT [7]		ICCVW2019	DeepLabv3	4.90	7.80	5.70	7.15	3.67	5.50
MiB [8]		CVPR2020	DeepLabv3	34.22	13.50	29.29	12.25	13.09	12.65
PLOP [28]		CVPR2021	DeepLabv3	65.12	21.11	54.64	44.03	15.51	30.45
UCD+PLOP [31]		TPAMI2022	DeepLabv3	66.30	21.60	55.10	42.30	28.30	35.30
REMINDER [32]		CVPR2022	DeepLabv3	68.30	27.23	58.52	-	-	-
RCIL [29]		CVPR2022	DeepLabv3	70.60	23.70	59.40	55.40	15.10	34.30
SPPA [33]		ECCV2022	DeepLabv3	66.20	23.30	56.00	-	-	-
CAF [34]		TMM2022	DeepLabv3	55.70	14.10	45.30	-	-	-
AWT+MiB [35]		WACV2023	DeepLabv3	59.10	17.20	49.10	33.20	18.00	26.00
EFW+MiB [36]		CVPR2023	DeepLabv3	78.00	25.50	65.50	56.00	16.70	37.30
GSC [37]		TMM2024	DeepLabv3	72.10	24.40	60.80	50.60	17.30	34.70
SegACIL(Ours)			DeepLabv3	79.16	38.00	69.36	75.02	41.20	58.91
<i>offline</i>		-	DeepLabv3	79.77	72.35	77.43	78.41	76.35	77.43

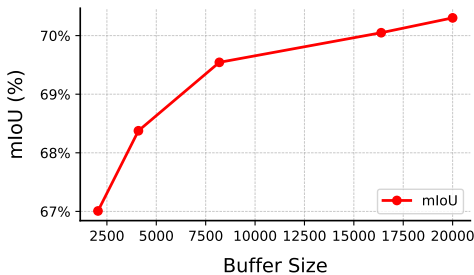


Fig. 2. Sequential 15-1 setting with different buffer size values.

Regularization Term Analysis. In the sequential 15-1 setting, we fixed the buffer size to 8192 and chose different values for γ . From Table III, it can be observed that the model is robust to the γ parameter, as the mIoU varies only slightly. This indicates that extensive parameter tuning for γ is unnecessary.

Pseudo-labels Threshold Analysis. In the overlap 10-1 setting, we fix the buffer size to 8192 and γ to 1, and select different threshold values. As shown in Table IV, smaller thresholds

TABLE III
SEQUENTIAL 15-1 SETTING WITH DIFFERENT γ VALUES.

γ	0-10	11-21	all
0.01	0.780613	0.411548	0.692741
0.1	0.780613	0.411548	0.692741
1	0.781369	0.420454	0.695437
10	0.780613	0.411538	0.692738
100	0.780615	0.411456	0.692720

such as 0.6 perform better, while larger values like 0.8 result in poorer performance, which is almost equivalent to having no pseudo-labels. This is because higher thresholds filter out the majority of pseudo-labels.

V. CONCLUSION

In this paper, we propose SegACIL, an analytic learning-based method to address the stability-plasticity dilemma in CSS. Our approach achieves performance equivalent to joint learning. Experiments of the three settings (sequential, disjoint,

TABLE IV

THRESHOLD VALUES ON THE OVERLAP 10-1 SETTING AND W/O MEANS NO PSEUDO-LABELS ARE USED.

τ	0-10	11-21	all
0.6	0.750170	0.412011	0.589142
0.7	0.733776	0.370846	0.560952
0.8	0.719293	0.352994	0.544865
0.9	0.719273	0.352995	0.544855
w/o	0.718298	0.361908	0.548588

and overlap) on the Pascal VOC2012 dataset demonstrate SegACIL's superior performance, offering a groundbreaking solution for CSS.

REFERENCES

- [1] V. M. Souza, D. M. dos Reis, A. G. Maletzke, and G. E. Batista, "Challenges in benchmarking stream learning algorithms with real-world data," *Data Mining and Knowledge Discovery*, vol. 34, no. 6, pp. 1805–1858, 2020.
- [2] T. Khan, W. Tian, G. Zhou, S. Ilager, M. Gong, and R. Buyya, "Machine learning (ml)-centric resource management in cloud computing: A review and future directions," *Journal of Network and Computer Applications*, vol. 204, p. 103405, 2022.
- [3] B. Yuan and D. Zhao, "A survey on continual semantic segmentation: Theory, challenge, method and application," *IEEE Transactions on Pattern Analysis & Machine Intelligence*, vol. 46, no. 12, pp. 10891–10910, Dec. 2024.
- [4] L. Wang, X. Zhang, H. Su, and J. Zhu, "A comprehensive survey of continual learning: Theory, method and application," *IEEE Transactions on Pattern Analysis and Machine Intelligence*, vol. 46, no. 8, pp. 5362–5383, 2024.
- [5] Z. Li and D. Hoiem, "Learning without forgetting," *IEEE transactions on pattern analysis and machine intelligence*, vol. 40, no. 12, pp. 2935–2947, 2017.
- [6] C. Peng, K. Zhao, and B. C. Lovell, "Faster ilod: Incremental learning for object detectors based on faster rcnn," *Pattern recognition letters*, vol. 140, pp. 109–115, 2020.
- [7] U. Michieli and P. Zanuttigh, "Incremental learning techniques for semantic segmentation," in *2019 IEEE/CVF International Conference on Computer Vision Workshop (ICCVW)*, 2019, pp. 3205–3212.
- [8] F. Cermelli, M. Mancini, S. R. Bulò, E. Ricci, and B. Caputo, "Modeling the background for incremental learning in semantic segmentation," in *Proceedings of the IEEE/CVF Conference on Computer Vision and Pattern Recognition*, 2020, pp. 9233–9242.
- [9] Y. Qiu, Y. Shen, Z. Sun, Y. Zheng, X. Chang, W. Zheng, and R. Wang, "SATS: Self-attention transfer for continual semantic segmentation," *Pattern Recognition*, vol. 138, p. 109383, 2023.
- [10] D. Baek, Y. Oh, S. Lee, J. Lee, and B. Ham, "Decomposed knowledge distillation for class-incremental semantic segmentation," *Advances in Neural Information Processing Systems*, vol. 35, pp. 10380–10392, 2022.
- [11] D. Goswami, R. Schuster, J. van de Weijer, and D. Stricker, "Attribution-aware weight transfer: A warm-start initialization for class-incremental semantic segmentation," in *Proceedings of the IEEE/CVF Winter Conference on Applications of Computer Vision*, 2023, pp. 3195–3204.
- [12] L. Zhu, T. Chen, J. Yin, S. See, and J. Liu, "Continual semantic segmentation with automatic memory sample selection," in *Proceedings of the IEEE/CVF Conference on Computer Vision and Pattern Recognition*, 2023, pp. 3082–3092.
- [13] Z. Yu, W. Yang, X. Xie, and Z. Shi, "TIKP: Text-to-image knowledge preservation for continual semantic segmentation," in *Proceedings of the AAAI Conference on Artificial Intelligence*, vol. 38, no. 15, 2024, pp. 16596–16604.
- [14] J. Tapon and A. van Schaik, "Learning the pseudoinverse solution to network weights," *Neural Networks*, vol. 45, pp. 94–100, 2013.
- [15] H. Zhuang, Z. Weng, H. Wei, R. Xie, K.-A. Toh, and Z. Lin, "ACIL: Analytic class-incremental learning with absolute memorization and privacy protection," in *Advances in Neural Information Processing Systems*, vol. 35. Curran Associates, Inc., 2022, pp. 11602–11614.
- [16] H. Zhuang, R. He, K. Tong, Z. Zeng, C. Chen, and Z. Lin, "DS-AL: A dual-stream analytic learning for exemplar-free class-incremental learning," *Proceedings of the AAAI Conference on Artificial Intelligence*, vol. 38, no. 15, pp. 17237–17244, Mar. 2024.
- [17] H. Zhuang, Y. Chen, D. Fang, R. He, K. Tong, H. Wei, Z. Zeng, and C. Chen, "GACL: Exemplar-free generalized analytic continual learning," in *Advances in Neural Information Processing Systems*. Curran Associates, Inc., 2024.
- [18] K. Fan, J. Li, S. Lai, L. Lv, A. Liu, J. Tang, H. H. Song, Y. Yue, and H. Zhuang, "TS-ACL: A time series analytic continual learning framework for privacy-preserving and class-incremental pattern recognition," 2024. [Online]. Available: <https://arxiv.org/abs/2410.15954>
- [19] H. Zhuang, Z. Weng, R. He, Z. Lin, and Z. Zeng, "GKEAL: Gaussian kernel embedded analytic learning for few-shot class incremental task," in *Proceedings of the IEEE/CVF Conference on Computer Vision and Pattern Recognition (CVPR)*, 2023, pp. 7746–7755.
- [20] H. Zhuang, D. Fang, K. Tong, Y. Liu, Z. Zeng, X. Zhou, and C. Chen, "Online analytic exemplar-free continual learning with large models for imbalanced autonomous driving task," *IEEE Transactions on Vehicular Technology*, pp. 1–10, 2024.
- [21] D. Fang, Y. Zhu, Z. Lin, C. Chen, Z. Zeng, and H. Zhuang, "AIR: Analytic imbalance rectifier for continual learning," aug 2024. [Online]. Available: <https://arxiv.org/abs/2408.10349>
- [22] H. Zhuang, R. He, K. Tong, D. Fang, H. Sun, H. Li, T. Chen, and Z. Zeng, "Analytic federated learning," 2024. [Online]. Available: <https://arxiv.org/abs/2405.16240>
- [23] Z. Liu, C. Du, W. S. Lee, and M. Lin, "Locality sensitive sparse encoding for learning world models online," in *The Twelfth International Conference on Learning Representations*, May 2024.
- [24] M. Everingham, S. A. Eslami, L. Van Gool, C. K. Williams, J. Winn, and A. Zisserman, "The pascal visual object classes challenge: A retrospective," *International journal of computer vision*, vol. 111, pp. 98–136, 2015.
- [25] Z. Li and D. Hoiem, "Learning without forgetting," *IEEE transactions on pattern analysis and machine intelligence*, vol. 40, no. 12, pp. 2935–2947, 2017.
- [26] M. Klingner, A. Bär, P. Donn, and T. Fingscheidt, "Class-incremental learning for semantic segmentation re-using neither old data nor old labels," in *2020 IEEE 23rd international conference on intelligent transportation systems (ITSC)*. IEEE, 2020, pp. 1–8.
- [27] U. Michieli and P. Zanuttigh, "Continual semantic segmentation via repulsion-attraction of sparse and disentangled latent representations," in *Proceedings of the IEEE/CVF conference on computer vision and pattern recognition*, 2021, pp. 1114–1124.
- [28] A. Douillard, Y. Chen, A. Dapogny, and M. Cord, "Plop: Learning without forgetting for continual semantic segmentation," in *Proceedings of the IEEE/CVF conference on computer vision and pattern recognition*, 2021, pp. 4040–4050.
- [29] C.-B. Zhang, J.-W. Xiao, X. Liu, Y.-C. Chen, and M.-M. Cheng, "Representation compensation networks for continual semantic segmentation," in *Proceedings of the IEEE/CVF Conference on Computer Vision and Pattern Recognition*, 2022, pp. 7053–7064.
- [30] J. Kirkpatrick, R. Pascanu, N. Rabinowitz, J. Veness, G. Desjardins, A. A. Rusu, K. Milan, J. Quan, T. Ramalho, A. Grabska-Barwinska, D. Hassabis, C. Clopath, D. Kumaran, and R. Hadsell, "Overcoming catastrophic forgetting in neural networks," *Proceedings of the National Academy of Sciences*, vol. 114, no. 13, pp. 3521–3526, 2017.
- [31] G. Yang, E. Fini, D. Xu, P. Rota, M. Ding, M. Nabi, X. Alameda-Pineda, and E. Ricci, "Uncertainty-aware contrastive distillation for incremental semantic segmentation," *IEEE Transactions on Pattern Analysis and Machine Intelligence*, vol. 45, no. 2, pp. 2567–2581, 2022.
- [32] M. H. Phan, S. L. Phung, L. Tran-Thanh, A. Bouzerdoum *et al.*, "Class similarity weighted knowledge distillation for continual semantic segmentation," in *Proceedings of the IEEE/CVF Conference on Computer Vision and Pattern Recognition*, 2022, pp. 16866–16875.
- [33] Z. Lin, Z. Wang, and Y. Zhang, "Continual semantic segmentation via structure preserving and projected feature alignment," in *European Conference on Computer Vision*. Springer, 2022, pp. 345–361.
- [34] J. Kirkpatrick, R. Pascanu, N. Rabinowitz, J. Veness, G. Desjardins, A. A. Rusu, K. Milan, J. Quan, T. Ramalho, A. Grabska-Barwinska *et al.*, "Overcoming catastrophic forgetting in neural networks," *Proceedings of the national academy of sciences*, vol. 114, no. 13, pp. 3521–3526, 2017.
- [35] D. Goswami, R. Schuster, J. van de Weijer, and D. Stricker, "Attribution-aware weight transfer: A warm-start initialization for class-incremental semantic segmentation," in *Proceedings of the IEEE/CVF Winter Conference on Applications of Computer Vision*, 2023, pp. 3195–3204.
- [36] J.-W. Xiao, C.-B. Zhang, J. Feng, X. Liu, J. van de Weijer, and M.-M. Cheng, "Endpoints weight fusion for class incremental semantic segmentation," in *Proceedings of the IEEE/CVF Conference on Computer Vision and Pattern Recognition*, 2023, pp. 7204–7213.
- [37] W. Cong, Y. Cong, J. Dong, G. Sun, and H. Ding, "Gradient-semantic compensation for incremental semantic segmentation," *IEEE Transactions on Multimedia*, vol. 26, pp. 5561–5574, 2024.

A. Proof of Theorem 1

Proof. At phase $t - 1$, we have

$$\hat{\Phi}_{t-1} = (\mathbf{U}_{1:t-2}^{(E)} \mathbf{U}_{1:t-2}^{(E)} + \mathbf{U}_{t-1}^{(E)\top} \mathbf{U}_{1:t-1}^{(E)} + \gamma \mathbf{I})^{-1} [\mathbf{U}_{1:t-1}^{(E)} \mathbf{V}_{1:t-2}^{\text{train}} + \mathbf{U}_{t-1}^{(E)\top} \dot{\mathbf{V}}_{t-1}^{\text{train}} \quad \mathbf{U}_{t-1}^{(E)\top} \ddot{\mathbf{V}}_{t-1}^{\text{train}}]. \quad (16)$$

Hence, at phase t , we have

$$\hat{\Phi}_t = (\mathbf{U}_{1:t-1}^{(E)} \mathbf{U}_{1:t-1}^{(E)} + \mathbf{U}_t^{(E)\top} \mathbf{U}_t^{(E)} + \gamma \mathbf{I})^{-1} [\mathbf{U}_{1:t-1}^{(E)} \mathbf{V}_{1:t-1}^{(E)} + \mathbf{U}_t^{(E)\top} \dot{\mathbf{V}}_t^{\text{train}} \quad \mathbf{U}_t^{(E)\top} \ddot{\mathbf{V}}_t^{\text{train}}]. \quad (17)$$

We have defined the autocorrelation memory matrix Ψ_{t-1} in the paper via

$$\Psi_{t-1} = (\mathbf{U}_{1:t-2}^{(E)} \mathbf{U}_{1:t-2}^{(E)} + \mathbf{U}_{t-1}^{(E)\top} \mathbf{U}_{t-1}^{(E)} + \gamma \mathbf{I})^{-1}. \quad (18)$$

To facilitate subsequent calculations, here we also define a cross-correlation matrix \mathbf{Q}_{t-1} , i.e.,

$$\mathbf{Q}_{t-1} = [\mathbf{U}_{1:t-1}^{(E)} \mathbf{V}_{1:t-2}^{\text{train}} + \mathbf{U}_{t-1}^{(E)\top} \dot{\mathbf{V}}_{t-1}^{\text{train}} \quad \mathbf{U}_{t-1}^{(E)\top} \ddot{\mathbf{V}}_{t-1}^{\text{train}}]. \quad (19)$$

Thus we can rewrite Eqn (16) as

$$\hat{\Phi}_{t-1} = \Psi_{t-1} \mathbf{Q}_{t-1}. \quad (20)$$

Therefore, at phase t we have

$$\hat{\Phi}_t = \Psi_t \mathbf{Q}_t. \quad (21)$$

From Eqn (18), we can recursively calculate Ψ_t from Ψ_{t-1} , i.e.,

$$\Psi_t = \left(\Psi_{t-1}^{-1} + \mathbf{U}_t^{(E)\top} \mathbf{U}_t^{(E)} \right)^{-1}. \quad (22)$$

Hence, Ψ_t can be recursively updated using its last-phase counterpart Ψ_{t-1} and data from the current phase (i.e., $\mathbf{U}_t^{(E)}$). This proves the recursive calculation of the autocorrelation memory matrix.

Next, we derive the recursive formulation of $\hat{\Phi}_t$. To this end, we also recurse the cross-correlation matrix \mathbf{Q}_t at phase t , i.e.,

$$\mathbf{Q}_t = [\mathbf{U}_{1:t-1}^{(E)} \mathbf{Y}_{1:t-1}^{(E)} + \mathbf{U}_t^{(E)\top} \dot{\mathbf{V}}_t^{\text{train}} \quad \mathbf{U}_t^{(E)\top} \ddot{\mathbf{V}}_t^{\text{train}}] = \mathbf{Q}'_{t-1} + [\mathbf{U}_t^{(E)\top} \dot{\mathbf{V}}_t^{\text{train}} \quad \mathbf{U}_t^{(E)\top} \ddot{\mathbf{V}}_t^{\text{train}}], \quad (23)$$

where

$$\mathbf{Q}'_{t-1} = \begin{cases} [\mathbf{Q}_{t-1} & \mathbf{0}_{d_{(E)} \times (d_{C_t} - d_{C_{t-1}})}], & d_{C_t} > d_{C_{t-1}} \\ \mathbf{Q}_{t-1}, & d_{C_t} = d_{C_{t-1}} \end{cases}. \quad (24)$$

Note that the concatenation in Eqn (24) is due to the assumption that $\mathbf{V}_{1:t}^{\text{train}}$ at phase t contains more data classes (hence more columns) than $\mathbf{V}_{1:t-1}^{\text{train}}$. It is possible that there are no new classes appear at phase t , then $\ddot{\mathbf{V}}_t^{\text{train}}$ should be $\mathbf{0}$.

Similar to what Eqn (24) does,

$$\hat{\Phi}_{(t-1)'} = \begin{cases} [\hat{\Phi}_{t-1} & \mathbf{0}_{d_{(E)} \times (d_{C_t} - d_{C_{t-1}})}], & d_{C_t} > d_{C_{t-1}} \\ \hat{\Phi}_{t-1}, & d_{C_t} = d_{C_{t-1}} \end{cases}. \quad (25)$$

We have

$$\hat{\Phi}_{(t-1)'} = \Psi_{t-1} \mathbf{Q}'_{t-1}. \quad (26)$$

Hence, $\hat{\Phi}_t$ can be rewritten as

$$\begin{aligned} \hat{\Phi}_t &= \Psi_t \mathbf{Q}_t \\ &= \Psi_t (\mathbf{Q}'_{t-1} + [\mathbf{U}_t^{(E)\top} \dot{\mathbf{V}}_t^{\text{train}} \quad \mathbf{U}_t^{(E)\top} \ddot{\mathbf{V}}_t^{\text{train}}]) \\ &= \Psi_t \mathbf{Q}'_{t-1} + \Psi_t \mathbf{U}_t^{(E)\top} [\dot{\mathbf{V}}_t^{\text{train}} \quad \ddot{\mathbf{V}}_t^{\text{train}}]. \end{aligned} \quad (27)$$

By substituting Eqn (26) into $\Psi_t \mathbf{Q}'_{t-1}$, we have

$$\begin{aligned} \Psi_t \mathbf{Q}'_{t-1} &= \Psi_{t-1} \mathbf{Q}'_{t-1} - \Psi_{t-1} \mathbf{U}_t^{(E)\top} (\mathbf{I} + \mathbf{U}_t^{(E)} \Psi_{t-1} \mathbf{U}_t^{(E)\top})^{-1} \mathbf{U}_t^{(E)} \Psi_{t-1} \mathbf{Q}'_{t-1} \\ &= \hat{\Phi}_{(t-1)'} - \Psi_{t-1} \mathbf{U}_t^{(E)\top} (\mathbf{I} + \mathbf{U}_t^{(E)} \Psi_{t-1} \mathbf{U}_t^{(E)\top})^{-1} \mathbf{U}_t^{(E)} \hat{\Phi}_{(t-1)'}. \end{aligned} \quad (28)$$

To simplify this equation, let $\mathbf{K}_t = (\mathbf{I} + \mathbf{U}_t^{(E)} \boldsymbol{\Psi}_{t-1} \mathbf{U}_t^{(E)\top})^{-1}$. Since

$$\mathbf{I} = \mathbf{K}_t \mathbf{K}_t^{-1} = \mathbf{K}_t (\mathbf{I} + \mathbf{U}_t^{(E)} \boldsymbol{\Psi}_{t-1} \mathbf{U}_t^{(E)\top}),$$

we have $\mathbf{K}_t = \mathbf{I} - \mathbf{K}_t \mathbf{U}_t^{(E)} \boldsymbol{\Psi}_{t-1} \mathbf{U}_t^{(E)\top}$. Therefore,

$$\begin{aligned} & \boldsymbol{\Psi}_{t-1} \mathbf{U}_t^{(E)\top} (\mathbf{I} + \mathbf{U}_t^{(E)} \boldsymbol{\Psi}_{t-1} \mathbf{U}_t^{(E)\top})^{-1} \\ &= \boldsymbol{\Psi}_{t-1} \mathbf{U}_t^{(E)\top} \mathbf{K}_t \\ &= \boldsymbol{\Psi}_{t-1} \mathbf{U}_t^{(E)\top} (\mathbf{I} - \mathbf{K}_t \mathbf{U}_t^{(E)} \boldsymbol{\Psi}_{t-1} \mathbf{U}_t^{(E)\top}) \\ &= (\boldsymbol{\Psi}_{t-1} - \boldsymbol{\Psi}_{t-1} \mathbf{U}_t^{(E)\top} \mathbf{K}_t \mathbf{U}_t^{(E)} \boldsymbol{\Psi}_{t-1}) \mathbf{U}_t^{(E)\top} \\ &= \boldsymbol{\Psi}_t \mathbf{U}_t^{(E)\top}. \end{aligned} \tag{29}$$

Substituting Eqn (29) into Eqn (28), $\boldsymbol{\Psi}_t \mathbf{Q}'_{t-1}$ can be written as

$$\boldsymbol{\Psi}_t \mathbf{Q}'_{t-1} = \hat{\boldsymbol{\Phi}}_{(t-1)'} - \boldsymbol{\Psi}_t \mathbf{U}_t^{(E)\top} \mathbf{U}_t^{(E)} \hat{\boldsymbol{\Psi}}_{(t-1)'}. \tag{30}$$

Substituting Eqn (30) into Eqn (27) implies that

$$\begin{aligned} \hat{\boldsymbol{\Phi}}_t &= \hat{\boldsymbol{\Phi}}_{(t-1)'} - \boldsymbol{\Psi}_t \mathbf{U}_t^{(E)\top} \mathbf{U}_t^{(E)} \hat{\boldsymbol{\Phi}}_{(t-1)'} + \boldsymbol{\Psi}_t \mathbf{U}_t^{(E)\top} [\dot{\mathbf{V}}_t^{\text{train}} \quad \dot{\mathbf{V}}_t^{\text{train}}] \\ &= [\hat{\boldsymbol{\Phi}}_{(t-1)'} - \boldsymbol{\Psi}_t \mathbf{U}_t^{(E)\top} \mathbf{U}_t^{(E)} \hat{\boldsymbol{\Phi}}_{(t-1)'} + \boldsymbol{\Psi}_t \mathbf{U}_t^{(E)\top} \dot{\mathbf{V}}_t^{\text{train}} \quad \boldsymbol{\Psi}_t \mathbf{U}_t^{(E)\top} \dot{\mathbf{V}}_t^{\text{train}}] \end{aligned} \tag{31}$$

which completes the proof. □